Biochemistry

 Volume 39, Number 40 October 10, 2000

Current Topics

Mechanism of Transmembrane Signaling: Insulin Binding and the Insulin Receptor†

F. P. Ottensmeyer,‡ Daniel R. Beniac,‡ Robert Z.-T. Luo,§ and Cecil C. Yip*,||

Ontario Cancer Institute and Department of Medical Biophysics, University of Toronto, Toronto, Ontario M5G 2M9, Canada, M. D. Anderson Cancer Center, Houston, Texas 77030, and Banting and Best Department of Medical Research, University of Toronto, Toronto, Ontario M5G 1L6, Canada

Received July 10, 2000

ABSTRACT: Transmembrane signaling via receptor tyrosine kinases generally requires oligomerization of receptor monomers, with the formation of ligand-induced dimers or higher multimers of the extracellular domains of the receptors. Such formations are expected to juxtapose the intracellular kinase domains at the correct distances and orientations for transphosphorylation. For receptors of the insulin receptor family that are constitutively dimeric, or those that form noncovalent dimers without ligands, the mechanism must be more complex. For these, the conformation must be changed by the ligand from one that prevents activation to one that is permissive for kinase phosphorylation. How the insulin ligand accomplishes this action has remained a puzzle since the discovery of the insulin receptor over 2 decades ago, primarily because membrane proteins in general have been refractory to structure determination by crystallography. However, high-resolution structural evidence on individual separate subdomains of the insulin receptor and of analogous proteins has been obtained. The recently solved quaternary structure of the complete dimeric insulin receptor in the presence of insulin has now served as the structural envelope into which such individual domains were fitted. The combined structure has provided answers on the details of insulin/receptor interactions in the binding site and on the mechanism of transmembrane signaling of this covalent dimer. The structure explains many observations on the behavior of the receptor, from greater or lesser binding of insulin and its variants, point and deletion mutants of the receptor, to antibody-binding patterns, and to the effects on basal and insulin-stimulated autophosphorylation under mild reducing conditions.

Cell−cell communication in multicellular organisms is crucial to the coordination of their physiological function. For such an interaction to occur at a distance, signaling ligand molecules are secreted by one type of cell and bind to specific surface receptor molecules on appropriate target cells. These cell surface receptors take on the role of transducers in the cell membrane which initiate the signal cascade that results in the cellular response of the target. For many ligand/receptor pairs the extracellular interaction with the receptor has been studied with atomic detail by crystallography, as have downstream intracellular signaling events. However, the difficulties of obtaining the structure for complete membrane-spanning receptor complexes have inhibited our understanding of the mechanism of this first event, of transmembrane signaling. Recently, the three-dimensional

† This work was supported by funds from the Medical Research Council of Canada and the National Science and Engineering Council of Canada and from Cancer Care Ontario.

* Address correspondence to this author. Telephone: 416-978-5150. Fax: 416-978-5568. E-mail: cecil.yip@utoronto.ca.

‡ Ontario Cancer Institute and Department of Medical Biophysics, University of Toronto.

§ M. D. Anderson Cancer Center, Houston.

|| Banting and Best Department of Medical Research, University of Toronto.

10.1021/bi0015921 CCC: $19.00
Published on Web 09/14/2000

quaternary structure of the entire insulin receptor complexed with insulin has been obtained by electron microscopy (*1*). In combination with the structures of insulin and of individual subdomains of the receptor solved at atomic resolution, the complex has now not only provided details of insulin binding but also illuminated the mechanism of transmembrane signaling.

The existence of a membrane receptor specific for insulin in insulin action was postulated some 30 years ago (*2*−*4*). The first experimental evidence directly demonstrating such an insulin-specific receptor protein was obtained in 1978 by photoaffinity labeling (*5*). In 1985 the primary structure of the insulin receptor was elucidated (*6*, *7*). The insulin receptor belongs to the superfamily of transmembrane receptor tyrosine kinases (TKs) (*8*) which include the monomeric receptors of the epidermal growth factor (EGF), of the platelet-derived growth factor (PDGF), of erythropoietin (Epo), of vascular endothelial growth factor (VEGF), and of fibroblast growth factor (FGF) and close to 10 other receptor TK families (*9*, *10*). In contrast, the insulin receptor (IR) is an intrinsic disulfide-linked dimer of heterodimeric disulfide-linked proteins of the form $(\alpha\beta)_2$, as are its homologues IGF-1R (insulin-like growth factor 1 receptor) and IRR (insulin receptor-related receptor) (*8*, *11*). Each IR α subunit of the $\alpha\beta$ monomer has a molecular mass of 135 kDa; each β subunit, 95 kDa. The α subunits are entirely extracellular, whereas the β subunits contain an extracellular portion, a transmembrane domain, and an intracellular part that includes a TK domain.

Monomeric receptor TKs are inactive but are activated by the extracellular binding of ligand which induces a noncovalent oligomerization that results in autophosphorylation of the intracellular TK domains. For many of these receptors, such as the EGF and FGF receptors, ligand binding induces receptor dimerization for activation (*12*−*18*). Threefold receptor complexes are formed by three monomeric units, such as the extracellular domains of DR5 (death receptor 5) that bind the trimeric TRAIL ligand (tumor necrosis factor-related apoptosis-inducing ligand) in crystals (*19*, *20*) and are thought also to do so in vivo for triggering of apoptosis. In contrast, the already covalently dimeric IR-like receptors are inactive without ligand and are activated by ligand binding without further oligomerization. Thus the structure of the dimeric IR receptor must inhibit the activation of its TK in the absence of insulin and permit the activation upon binding of this ligand. Many authors, such as Taylor et al. (*21*), logically suggest a general mechanism in which an insulin-induced conformational change in the extracellular domain of the receptor causes the two receptor monomer halves to move closer together and, in doing so, increases the receptor kinase activity via a conformational change in the intracellular domain. However, how the addition of insulin to the receptor accomplishes these conformational changes was not known, since the quaternary structure of the IR dimer had not been solved, and high-resolution detail was available only for several unconnected subdomains of the receptor based on crystallography or modeling of highly analogous domains (*22*−*25*).

The quaternary structure of the insulin-bound IR dimer complex was solved by 3D reconstruction from scanning transmission electron micrographs. The structure showed that binding of a single insulin molecule results in a conformation indicative of IR dimer activation by transphosphorylation (*1*). In addition, the crystallographic structure of the N-terminal domains of the IGF-1 receptor has become available (*26*), permitting now the docking of the exact or highly analogous atomic structures of virtually all subdomains of IR into the quaternary structure of the complex. This has prompted a reexamination of the structural details of the interaction of insulin with the receptor and an elucidation of the mechanism of insulin signaling from extracellular binding to intracellular TK activation. It illuminates the crucial first step in the signal cascade initiated by insulin binding for its normal metabolic processes and for the multitude of insulin-related diseases.

Downstream Cascade

Despite the differences in the receptor TKs mentioned above, there is an almost bewildering similarity in the intracellular signaling pathways initiated by these proteins. For all receptor TKs, the binding of ligand to the extracellular domain leads to phosphorylation and activation of the tyrosine kinase in the cytoplasmic domain. This in turn activates a number of common downstream signaling molecules, such as phospholipase C-γ, phosphatidylinositol 3 (PI3) kinase, GTPase-activating protein, pp60c-src, p21ras, Raf-1 kinase, and MAP kinases (*9*).

For the EGF and PDGF receptors, intracellular signaling is mediated via the Src homology 2 (SH2) domains of adaptor and effector proteins that attach to specific phosphorylated tyrosine residues of the receptors (*27*). In contrast, intracellular insulin receptor signaling events are mediated primarily through the family of insulin receptor substrates (IRS), such as the 185 kDa protein IRS-1 with 20−22 potential tyrosine phosphorylation sites that in turn bind various SH2-containing downstream proteins (*28*). Such an interaction of IRS-1 with the PI3 kinase molecule leads to one of the diverging branches of the insulin signaling pathways believed to be critical for the increase in cellular glucose transport that occurs in response to insulin binding (*29*, *30*). This path includes the insulin regulatable glucose transporter (GLUT4) system and results in translocating GLUT4 proteins from a sequestered intracellular pool to the plasma membrane (*31*). A second insulin-activated pathway increases the enzymatic activity of glycogen synthase (*32*), while other metabolic effects include lipogenesis, lipolysis, and protein synthesis. Growth-promoting effects of insulin include DNA synthesis, cell division, and differentiation (reviewed in ref *9*).

With such a diverse network of insulin-mediated biological responses, it is not surprising that malfunctioning of the insulin signaling system would lead to the manifestation of a variety of physiological disorders or complications resulting from the development of diabetes, including neuropathy, nephropathy, retinopathy, and cardiovascular diseases. The insulin signaling system can be divided into three components: insulin and its production, the insulin receptor, and downstream elements coupled to the insulin receptor kinase. Normal carbohydrate metabolism is dependent on the complex and finely balanced interplay between the three components. The lack of insulin, due to the destruction of pancreatic β cell, leads to type 1 insulin-dependent diabetes. Type 2 diabetes, occurring in approximately 5% of North Americans, with a prevalence as high as 37% in some native

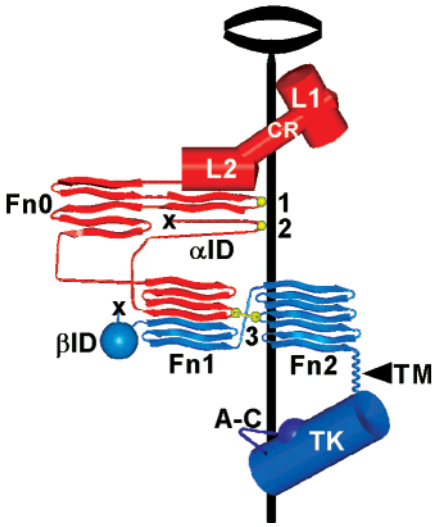

FIGURE 1: Sequential spatial arrangement of the subdomains of one αβ monomer of the insulin receptor deduced from the 3D structure (*1*). The N-terminus of the α subunit (red section) is at the top, and the C-terminus of the β subunit (blue section) is near the bottom. The domains and their delimiting amino acid sequences are as follows (*6*): αN-terminal−1−L1−158/159−cysteine rich (CR)−310/311−L2−470/471−fibronectin0 (Fn0)−572/573−αFn1−661/662−α-insert domain (ID)−719−αC-terminal; βN-terminal−724−βID−779/780−βFn1−816/817−βFn2−913/914−exterior juxtamembrane−929/930−transmembrane (TM)−952/953−interior juxtamembrane−977/978−tyrosine kinase (TK)−1283/1284−C-terminal region−1388−βC-terminal. Other important residues are Cys524 (denoted by 1), which forms an α−α bond on the 2-fold symmetry axis, as does one of Cys682, Cys683, or Cys685 (shown as 2). An α−β bond is formed by Cys647 in Fn1 of the α subunit and Cys872 in Fn2 of the β subunit (shown as 3). x marks the cleavage site between the α and β subunits in the proreceptor with the elimination of four amino acids. A−C denotes the catalytic loop and the activation loop [residues 1130−1137 and 1149−1170, respectively (*22*, *23*)].

populations (*33*), generally is the result of a combination of peripheral insulin resistance and defects in β-cell function. Recent advances from the use of transgenic mice to alter the expression of either the insulin receptor or specific members of the IRS family in a tissue-specific manner suggest the multisystem nature of insulin resistance that involves the insulin receptor and receptor-coupled downstream events (reviewed in ref *34*).

Insulin Receptor Structure

The domain structure of IR is shown for one αβ monomer in Figure 1 in a schematic representation that was derived from the 3D quaternary structure (*1*). The L1−Cys-rich−L2 domain structure has been solved by crystallography for the homologous IGF-1 receptor (*26*). The next three domains, fibronectin type III-like domains Fn0, Fn1, and Fn2, have been modeled after many such structures solved by NMR spectroscopy and crystallography (*24*, *25*, *35*). No other extracellular domain has been solved in detail. The seven-stranded beta-sandwich Fn1 domain links the two subunits, being composed of four beta strands from the α subunit and three from the β subunit and containing a covalent bond between the two subunits via Cys647 and Cys872. The C-terminal region of the α subunit, the α-insert domain, emerges from Fn1 at Phe662 and forms one of the two disulfide bonds that link corresponding αβ monomers. The other dimerizing α−α disulfide bond is formed between corresponding Fn0 domains. In the intracellular region of the β subunit only the TK domain structure has been solved both in the inactive form and when liganded with a peptide substrate (*22*, *23*).

Electron microscopic studies provided two-dimensional views of the IR ectodomain and of the entire IR complex that indicated X-, Y-, and V-shaped structures (*36*−*38*). The recent 3D reconstruction from scanning transmission electron cryomicroscopy of the insulin-bound IR dimer (*1*) indicated a roughly globular aspect within which the higher densities at different orientations provided a ready interpretation of the continuity and connectivity of the 2-fold symmetric structure (Figure 2). Moreover, different views of the higher density representations also indicated the presence X-, Y-, and V-shapes within either the ectodomain portion or the complete complex. The presence of bound insulin labeled with an easily visible gold marker permitted the identification and division of the structure into the ectodomain, the transmembrane region, and the intracellular component (*1*). This in turn suggested a logical structural domain sequence for the biochemical domains (Figures 1, 2, and 6b). The sequence assignment also readily explained the pattern of antibody binding observed by Tulloch et al. (*38*), in which pairs of antibodies to Fn0 and to the β-insert domain near Fn1 (near opposing ends of the reconstruction) provided a parallel line aspect, while the combination of antibodies to Fn0 and to the Cys-rich domain near the central region resulted in a cross-pattern for the antibodies on the dimer ectodomain.

The connectivity and the shape of the higher density structural elements have provided the potential of docking different atomic domains into the complete 3D reconstruction. Although the total structure was only at a resolution of 2.0 nm, the center of mass of different domains is defined to within about 0.2 nm, and the shape of the envelope provides a severe constraint to potential rotations in the fitting of asymmetric structures. Thus the atomic structures for Fn1 and Fn2 could be readily fitted into the reconstruction of the IR dimer, as could the TK domains (*1*). Moreover, the activation loops of the pair of TK domains were then in a position and at a distance to fit a bridging mass and reach the opposing domain for activation by transphosphorylation (see also Figures 5b and 6b).

Similarly, the recent monomeric structure of the L1−Cys-rich−L2 (LCL) domains of the analogous IGF-1 receptor has been fitted symmetrically into the dimeric reconstruction after adapting its sequence to the equivalent IR sequence. The fitted structure is shown in Figure 3, after several rounds of energy minimization calculations to eliminate atom clashes.

Insulin Binding Region

The fit of the two LCL regions forms a diamond-shaped central tunnel (Figure 3). In this arrangement the walls of the tunnel and its entrances are lined with almost all of the amino acids that have been linked to the binding of insulin (Table 1). The atomic structure of human insulin fits into this tunnel as shown in Figure 3 and detailed in the stereoview in Figure 4a, involving binding sites on both α monomers. Insulin proximity to one monomer juxtaposes

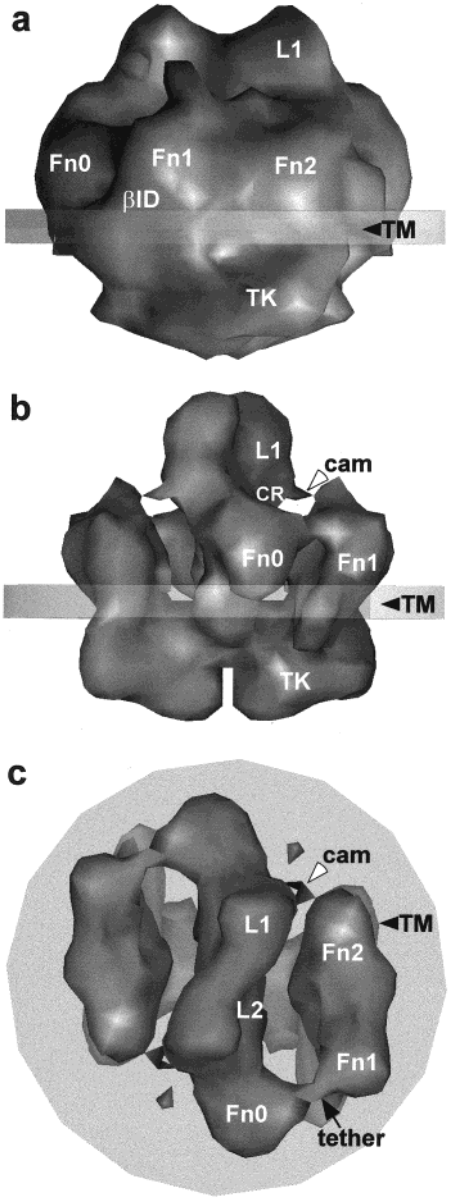

FIGURE 2: Three-dimensional structure of the human insulin receptor reconstructed from images of the purified dimeric insulin receptor complexed with insulin obtained via low dose scanning transmission cryomicroscopy (*1*). (a) Density threshold representation at 100% of the total volume showing roughly globular structure. The ectodomain region is in the upper half, above the transparent disk representing the approximate position of the cell membrane; intracellular domains are below. Regions of one $\alpha\beta$ monomer of the dimeric structure labeled as determined from insulin location, connectivity, mass distribution, and fitting with subdomains of known structures. The maximum diameter is 150 Å. (b and c) Density threshold at 85% of the total volume to show connectivity of structure. (b) View as seen in the plane of the membrane, rotated 90° about the vertical axis with respect to the view in (a). Labeling as in (a). (c) View as seen from the exterior of the cell, down the 2-fold symmetry axis of the $(\alpha\beta)_2$ heterodimer, with fainter regions of structure on the distal side of the membrane disk. Arrowheads (white) point to the cam-like feature (see text), and the arrow (black) points to the connecting tether. For domain abbreviations see Figure 1.

major hydrophobic areas on the insulin B chain and on L1, as well as charged amino acids with matching side chains on the CR and L2 regions (Table 1, Figure 4b). Interactions of insulin with the other monomer are predominantly electrostatic salt bridges, with no obvious hydrophobic components (Figure 4c). These interactions and others are listed in Table 1, with corresponding side chains rotated toward each other to a minimum of 2.5 Å where possible. Amino acids Arg14 and Ser323 of IR have been shown to affect insulin binding but are too distant in this structure for direct interactions with insulin, without water molecules to bridge the gap or potential hydrogen bond chains through other side chains (Table 1). However, these distances could be slightly smaller if the relative angles between the L1, CR, and L2 subdomains had not been kept constant during the adaptation of the LCL structure of the IGF-1R structure to the sequence of IR.

One constraint on the docking of insulin was the need to satisfy the location near L1 of the Nanogold label attached to PheB1 of insulin for electron microscopy (*1*). This requirement was easily satisfied by flexing the insulin B chain between amino acids 1−6, a motion that appears to occur naturally, as judged from different crystal structures of the molecule (*39*). In the crystal structure of human insulin the B-chain N-terminal amino acids lie against insulin in the direction toward the viewer (Figure 4a,b).

The components of the insulin binding tunnel are naturally arrayed such that the two L1−CR regions can readily separate by rotating toward the Fn1/Fn2 region of their own monomer. Insulin can bind to each LCL component in one of two orientations using one of two sets of binding sites as indicated in Table 1. Each of these orientations puts insulin in the correct position to bind to the complementary set of sites on the other unliganded monomer. Two insulin molecules might bind to the dimeric receptor in the open position, but high-affinity binding of insulin would involve both sets of sites in an insulin-induced closed position of the two monomers and would preclude the binding of a second insulin ligand.

Fibronectin and Insert Domain Linkers

The linkage in the ectodomain between the LCL regions and the IR transmembrane domain is via three fibronectin type III (Fn) domains and two insert domains of still unknown structure, one each on the α and β subunits of each monomer. This region also provides the two disulfide bonds that covalently link two α subunits to form the constitutive IR dimer (*40*). From considerations of symmetry of the $(\alpha\beta)_2$ dimer, the two α−α disulfide bonds occur one above the other on the 2-fold symmetry axis of the dimer (labeled 1 and 2, Figure 1).

Two of the Fn domains, Fn1 and Fn2, are not involved in dimer formation and have been modeled into the 3D reconstruction as the normal seven beta-strand fibronectin type III structure (*1*, *24*, *35*) (Figure 5). The α-insert domain (ID) is led from the Fn1 domain past Fn0 and the near side of the L2 domain to the diad axis of the dimer. Here it forms one of the α−α disulfide bonds with its symmetric partner insert domain (αID, Figure 5a). The location of the remaining 34 C-terminal amino acids of the α subunit is unknown, although the final 12−16 residues, which assist in insulin binding (*8*, *41*−*43*), must be near the centrally located insulin-binding site.

The structure of Fn0, designated CD in prior descriptions (*1*, *35*, *44*), is more problematical. The domain sequence of

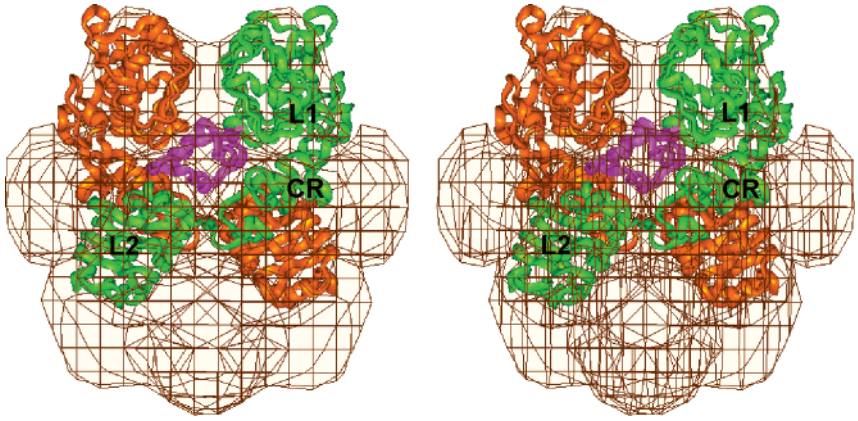

FIGURE 3: Side view (parallel stereo) of the IR dimer structure at the volume corresponding to total receptor mass, in wire mesh representation (brown), at a slight rotation compared to Figure 2a, fitted centrally with two LCL regions of IR as adapted with the IR sequence (*6*) and the coordinates of the corresponding IGF-1R structure (*26*). The amino acid backbone representation is shown as ribbons. One LCL monomer region is shown as green with LCL regions labeled; the other is shown as orange-brown. Insulin in backbone representation (fuchsia) is modeled into the diamond-shaped opening between the two LCL regions (enlarged in Figure 4a). Accession numbers: insulin [Protein Data Bank (PDB): 1BEN] (*65*); LCL structure (PDB: 1IGR) (*26*).

Table 1: Modeled Approaches between Insulin Side Chains and Insulin Receptor Side Chains[a]

insulin residue	insulin receptor residue (region)	inter-side-chain distance (Å)
	Monomer I	
GluA4[b]	Arg86 (L1)	2.5[c]
ThrA8		2.6
LysB29	Asp12 (L1)	2.6
	Asn34	2.5
GluA17	Arg331 (L2)	2.5
GlnA21	Ser323	5.3[d]
	Monomer II	
SerB9	Gln34 (L1)	2.8
HisB10	Arg14	5.0[d]
GluB13	Arg86	2.5
ValB12	Phe89 (L1)	2.5
LeuB17	Leu87	2.5
TyrB16	Leu87	2.5
PheB24	Phe88	2.5
TyrB26	Tyr91	3.5[d]
GluB21	His247 (CR)	2.5
	Asn249	2.5
ArgB22	Glu250	4.0[d]
	Glu287	2.5
	His247	2.5
AsnA5	Arg331 (L2)	2.5
AsnA15		2.5

[a] Individual amino acids in insulin designated as important in binding to the receptor are A1, A4, A5, A19, A21, B12, B16, B17, B24, B25, and B26 (*8*, *42*, *49*). On the insulin receptor amino acids found to be involved in insulin binding are 12, 14, 15, 34, 36, 39, 64, 86 89, 90, 91, 243−251, 323, and 707−716 (*41*, *48*−*50*, *56*, *57*, *60*); of these, only amino acids 707−716 are not in the L1−CR−L2 domains. [b] Potential vicinal interactions are grouped. [c] Minimum distance of approach modeled at 2.5 Å during side-chain rotations. [d] Closest approach; interaction would require a water molecule, a hydrogen bond chain, or a rotation of the entire L1 or L2 regions.

the quaternary structure (*1*) and the accessibility of Fn0/CD to monoclonal antibodies and Fab fragments (*35*, *45*) put Fn0 at the extreme ends of the central region of the IR ectodomain. However, the α−α disulfide bond at Cys524 within this region requires that this domain extend past L2 to the diad symmetry axis of the IR dimer. This is possible by rotating one surface hairpin loop in the Fn0 beta-sandwich configuration that contains Cys524 and two neighboring beta strands (Figures 1 and 5a). The additional size of this Fn region (122 amino acids versus 106 and 97 for Fn1 and Fn2, respectively) still provides enough mass to accommodate the volume of this region in the EM reconstruction.

The tyrosine kinase domains of the β subunits have been docked into the quaternary structure previously, as has the potential extension of the flexible TK activation loops (*1*, *19*). The complete set of fitted domains, plus insulin, is shown in Figure 5b. Unfilled mass still remains for the unknown structures of the C-terminal β domain and for the βID region at the N-terminal of the βFn1 domain, e.g., below Fn1 in Figure 2b.

Physical Model and Mechanism for Transmembrane Signaling

In contrast to activation of monomeric membrane receptors, activation of the IR tyrosine kinase cannot be caused by ligand-induced dimerization, since IR is covalently dimeric. Some monomeric receptors may form spontaneous noncovalent dimers prior to ligand binding, as suggested recently by the crystal structure of the ectodomains of the erythropoietin receptor EpoR (*46*). For these, a scissor-like mechanism has been invoked for TK activation. However, the articulated structural features of the IR dimer indicate a different mechanism.

Figure 2c shows that the central, extracellular region of the two sets of contiguous domains from L1 to Fn0 is flanked on both sides by the pontoon-like Fn1/Fn2 domains, each of which is tethered near one end only between Fn1 and Fn0. The two Fn2 ends, which terminate at the juxtamembrane and transmembrane (TM) domains, are separated from the central regions by the bumper-like cam structures of the two symmetry-related CR domains, which abut the top portion of the Fn2 domains (Figures 2 and 6b). This separation affects the positions of the TM domains and also of the intracellular TK domains which are joined to them.

Nuclear magnetic resonance spectroscopy has shown that helical TM domains of the epidermal growth factor receptor, similar to the IR TMs, cannot transmit signals along their lengths; at most, a torsional force can be exerted by them

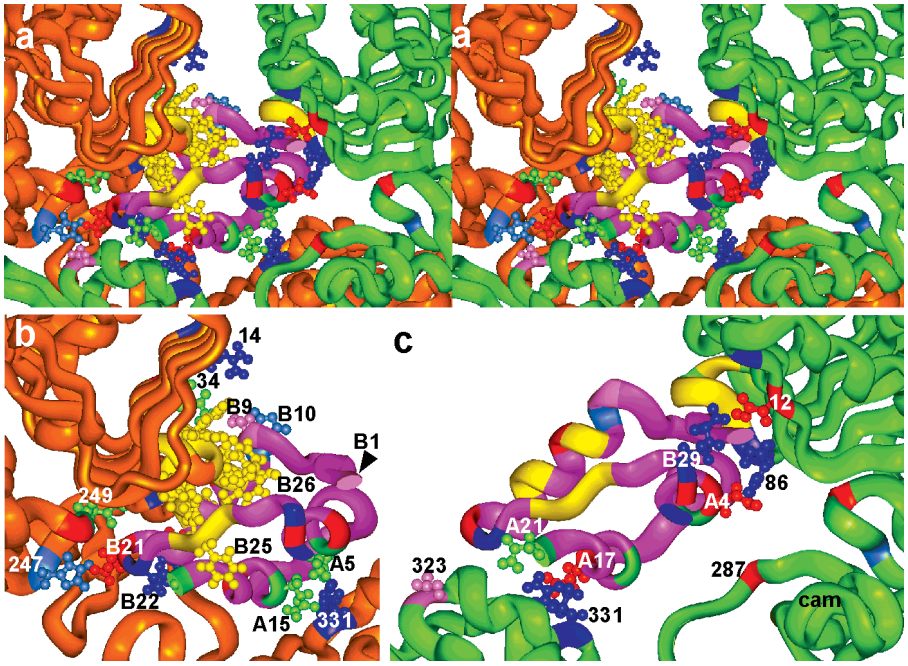

FIGURE 4: Detail of the insulin interaction with IR. (a) View (parallel stereo) of the IR insulin-binding region of docked LCL regions (orange-brown and green) fitted with insulin (fuchsia). The backbone representation except for amino acid side chains tabulated in Table 1. Dark blue side chains and backbones indicate positive charge; red, negative charge; turquoise, polarized or hydrogen bonding; yellow, hydrophobic side chains. See panels c and d and Table 1 for identification. (b) Potential contacts of insulin amino acids with one LCL monomer (orange-brown). Side chains are labeled according to insulin polypeptide chain A or B. Simple numbers refer to side chains of the LCL region. Most chains in the dense hydrophobic patches are not labeled. For distances of side chain pairs see Table 1 (monomer II). Color code as in panel a. (c) Insulin contacts with the second LCL monomer (green). Labels and color scheme as in panel a. For interactions see Table 1 (monomer I).

(*47*). However, these domains can shift laterally within the membrane. Such a shift of the TM regions provides a simple, controllable, and direct means for transmembrane signaling by IR.

The structural basis for IR signaling is modeled schematically in Figure 6c,d, pared to a two-dimensional representation. The open extracellular structure of the IR dimer (Figure 6c) is suggested from previous electron microscopic results of insulin-free IR ectodomains (*36*, *38*), suggesting that the two sets of L1−CR regions are splayed apart. The closed structure (Figure 6d) is based on the 3D reconstruction of insulin-bound IR (*1*).

In the inhibitory, insulin-free state (Figure 6c), a minimum separation is maintained between the two intracellular TKs, despite thermal motion of the two tethered Fn1/Fn2/TM domains, by the α-ectodomain CR cam regions that contact the Fn2/TM domains. Consequently, the distance between the intracellularly attached TKs prevents the flexible TK activation loop (*23*) of one TK from reaching the catalytic transphosphorylation site of the other TK.

High-affinity binding of a single insulin molecule joins the two LCL domains of the ectodomain (Figure 6d) against a small torsional resistance offered by the two on-axis disulfide bonds (1 and 2 in Figures 1 and 6c,d). This rotation also moves the cam protrusions upward, such that thermal motion can bring the pair of Fn2/TM-axle regions closer to the central region of the ectodomain. The reduction in separation between the TM axles permits a sufficiently close approach of the associated TK domains to allow transphosphorylation of the TK activation loops at the catalytic loci of each opposite TK, as suggested by the structure in Figure 6b. Docking of the TK structures indicated a separation of only 4 nm between opposite catalytic TK sites, sufficiently close to be accessed by opposing activation loops (*1*).

When insulin detaches from the receptor, the two L1−CR domains spring apart again, as the two strained Cys−Cys linkages return to their equilibrium positions (1 and 2, Figure 6c). At the same time the CR-region cams again restrict the approach of the TK domains, increasing their separation, possibly to facilitate downstream signaling actions via the 185 kDa IRS-1 molecule as well as eventual dephosphorylation.

The Model and Reality

The detailed model of insulin binding, the relative positioning of the known domain structures into the quaternary structure of the IR dimer, and the mechanism for transmembrane signal transduction as proposed here explain virtually every observation on the behavior of IR. Only a few examples are detailed here.

The Insulin Binding Site. A number of ligand/IR interactions change in character as either insulin or IR is modified. Experimentally, the interaction of insulin with the CR loop from 242 to 251 is strengthened by the CR mutations P**RR**YY**D**FQDW from P**PP**YY**H**FQDW, which create an additional positive charge in this region (*48*). In the modeled binding site, GluB21 of insulin is near the slightly positive His247 in the CR loop (Table 1), with a negatively charged Asp250 in the vicinity weakening the interaction. The mutation of His247Asp makes a direct interaction of Asp247 with ArgB22 possible, while the introduction of the positive charges from Arg243 and Arg244 provides a potential stronger electrostatic attraction to GluB21.

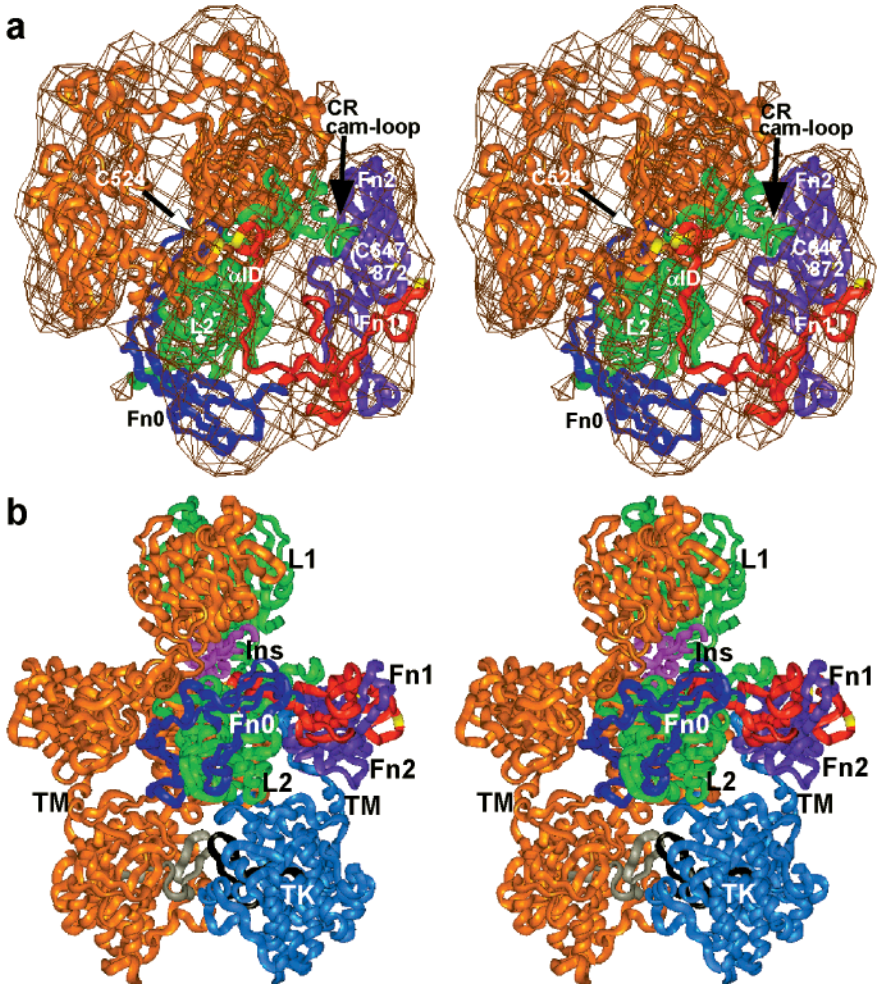

FIGURE 5: (a) Views of fibronectin domains (parallel stereo) docked into the ectodomain quaternary structure of IR. Fn0 and αID regions are modeled as extending around L2 to the 2-fold symmetry axis to form the two α−α disulfide bonds between the two IR αβ monomers. Domains of one αβ monomer are colored and labeled for identification, as are the α−β disulfide bond and one of the α−α disulfide bonds. For clarity, the LCL regions are shown only with part of the CR domain and all of the L2 domain (amino acids 250−470). (b) Fit of 14 domains plus insulin docked into 3D EM reconstruction of the quaternary structure of the IR dimer. The TM and juxtamembrane domains, of unknown structure, modeled as helix and loop structures are arbitrarily placed to connect the Fn and TK domains. The ectodomain has been raised slightly to show the TM domain positions more clearly. The unknown structures of the βID region at the N-terminus of the βFn1 domain and the C-terminal β-domains have not been modeled. Color scheme as in panel a. Activation loops in Tks are in black and silver. Accession numbers: modeled Fn0/Fn1/Fn2 (PDB: 1FNF) (*35*, *66*); TK structure (PDB: 1IRK) (*22*).

Experimentally, a mutation in Phe89 of the L1 domain reduces insulin binding (*49*). Phe89 forms part of a hydrophobic contact region between L1 and insulin (Table 1, Figure 4a,b), which would be weakened by any decrease in the size of this region.

A mutation of HisB10 in insulin to AspB10 creates a superactive insulin (*50*). In the binding site, HisB10 is close to Arg14 of L1 (Figure 4a,b). A stronger and closer ionic interaction with Arg14 would be expected with the introduction of the negatively charged side chain of aspartic acid in insulin at position B10.

The more potent insulin from urodeles has an Ala-Arg N-terminal extension and a Thr10His substitution in the A chain (*51*). The extension easily fits into the structure. Moreover, the additional Arg moiety can interact with the nearby Glu287 of the CR region (Figure 4c), while HisA10 (at the position of ThrA8 in human insulin) can reach Asp59 in L1 to potentiate binding. Conversely, the 10-fold lesser potency of guinea pig insulin (*52*) can be based in part on amino acid changes Leu(B17)Ser, Arg(B22)Asp, and Glu(A17)Asn, which weaken the interaction to Phe89, Glu287, and Arg331 of IR, respectively (Table 1). Only a partial compensation would be expected from the additionally changed Leu(A13)Arg in guinea pig insulin, which permits a new interaction between ArgA13 and Glu287.

Reduction of α−α *Disulfide Bonds*. High-affinity binding of insulin and also basal insulin-independent autophosphorylation are initially augmented and then diminished by reduction of the disulfides of IR with increasing concentrations of dithiothreitol (*53*). In the signal tranduction model (Figure 6c,d), normal high-affinity insulin binding must overcome a torsional energy barrier created by the binding-induced elastic strain in the two α−α disulfide bonds on the diad axis of the IR dimer. Reduction of one of the two disulfide bonds eliminates this torsional strain and facilitates high-affinity binding. Further reduction separates IR into monomers, abrogating high-affinity binding, which involves two α subunits in close proximity. Similarly, basal levels of transphosphorylation in the absence of insulin reflect the torsional resistance of the two on-axis disulfide bonds which tend to maintain the blocking cams in the insulin-free equilibrium position against random thermally induced

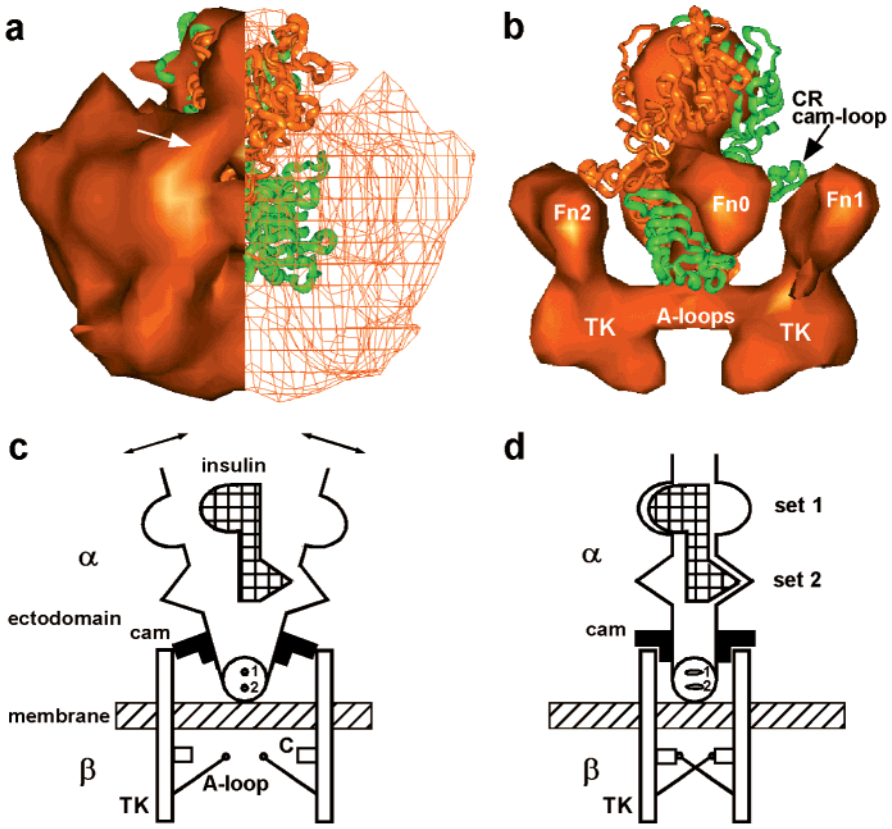

FIGURE 6: (a) End view of the full-mass representation of the IR dimer: left half, surface rendering; right half, wire mesh representation. Fitted structure of two IR-adapted LCL regions (green and orange-brown) showing correspondence of surface features and extent in uppermost regions (L1). Arrow: cam-like region on the CR domain. (b) Higher density solid surface representation of the view rotated slightly from panel a to show CR loop regions (cams) of atomic structure reaching the top portion of Fn2 domains of the 3D reconstruction (compare with top view in Figure 5a). (c and d) Simplified schematic of structural changes during activation of the insulin receptor. (c) Inhibitory state: ectodomain of dimeric α subunits each with two differing insulin binding sites and a blocking cam. Unbound bivalent insulin: *β* subunits resting against cams, crossing membrane, with tyrosine kinase (TK) domains separated. Abbreviations: A-loop, activation loop; C, catalytic region. Small on-axis circles (1 and 2) represent the two α−α disulfide bonds. Arrows indicate thermally induced motion. (d) Insulin bound state: blocking cams rotated and *β* subunits resting closer to the center of the ectodomain. TK domains are in position for transphosphorylation via A-loops (compare with panel b in this figure and Figure 5b). Sets 1 and 2 indicate schematically different sets of amino acids from monomers I and II (Table 1) interacting with corresponding different sites on insulin.

motion (Figure 6c). The breakage of one disulfide bond would remove the torsional resistance, resulting in a more frequent random approach of the TK domains for transphosphorylation. The reduction of both bonds would result in monomeric IR, halting transphosphorylation altogether.

The effect on insulin binding and TK transphosphorylation by deletions that include one of the α−α disulfide bonds is explained similarly (*54*).

Deletional Activation. The IR is activated artificially by removal of amino acids 1−578 through tryptic digestion (*55*). This cleavage still retains covalent links between the monomers and between the α and *β* subunits. However, the insulin-binding region and the CR domains have been removed, along with the CR cam structures that, in the model, block the approach of the Fn2 domains to central portions of the ectodomain. Thus the *β* domains and their TKs can move closer together and transphosphorylate, independent of insulin. A more limited deletion, which removes part of L2 and most of the CD region, activates IR and blunts the action of insulin (*54*). Such a deletion removes the physical support for the CR cam region of the partner monomer, thus partly collapsing the cam to permit the approach of the TK regions. At the same time the geometry of the insulin-binding site in the L2 and CR region would be affected, as well as the insulin-induced change in the relative configuration of the entire LCL regions.

Other aspects of the function of IR that can be explained by the arrangement of the domains in the 3D structure include the negative or positive cooperativity of binding of insulin to native or mutant receptors (*56*, *57*), the loss of intracellular TK activity from the extracellular Cys647Ser mutation (*8*), the impaired TK action by the Phe383Val and Asp919Glu mutations (*21*, *58*, *59*) which are near the cam and cam-contact regions, the effect on extracellular binding of insulin by the intracellular TK mutant Met1153Ile (*60*), the predominantly passive role of the transmembrane region (*61*−*63*), and the changes in downstream kinase activity between monomeric and dimeric IR (*64*).

Conclusions

The quaternary structure of IR, fitted with the atomic coordinates of highly analogous domains of IGF-1R substituted with the IR sequence, has resulted in a detailed description of the insulin-binding site on the insulin receptor both in the normal state and in the presence of mutations. Moreover, the combination of structural detail from the 20 Å electron microscopic structure of the entire IR dimer and

of atomic resolution from the crystal and NMR structures of IR domains yielded a self-consistent model for the mechanism of the initial phase of insulin action on extracellular binding to effect intracellular receptor tyrosine kinase activation.

The model is highly explanatory as well as predictive in terms of potentiating or diminishing insulin action by suitable mutations that affect the binding surfaces both in insulin and in IR. Moreover, it suggests that the signaling response can be affected as well, independent of insulin binding, by modifications in the cam region and in the linkages of the domains by mutations or appropriately designed ligands.

The model provides a simple mechanical paradigm for the reversible transmembrane signaling response. It explains the need for the complexity of structural components to control both inhibition and accommodation of tyrosine kinase activation. The model gives ready structural explanations for many normal effects, for various mutations, and for mild chemical reduction of the insulin receptor. It thus provides a comprehensive structural basis for the mechanics of transmembrane signal transduction for the intrinsically dimeric insulin-like membrane receptors and a comparative model for the action of the class of monomeric receptors, such as EpoR, that assemble as ligand-free preformed noncovalent dimers.

REFERENCES

1. Luo, R. Z.-T., Beniac, D. R., Fernandes, A. B., Yip, C. C., and Ottensmeyer, F. P. (1999) *Science 285*, 1077−1080.
2. House, P. D. R., and Wiedemann, M. J. (1970) *Biochem. Biophys. Res. Commun. 41*, 541−548.
3. Freychet, P., Roth, J., and Neville, D. M., Jr. (1971) *Proc. Natl. Acad. Sci. U.S.A. 68*, 1833−1837.
4. Cuatrecasas, P. (1971) *Proc. Natl. Acad. Sci. U.S.A. 68*, 1264−1268.
5. Yip, C. C., Yeung, C. W., and Moule, M. L. (1978) *J. Biol. Chem. 253*, 1743−1745.
6. Ebina, Y., Ellis, L., Jarnagin, K., Edery, M., Graf, L., Clauser, E., Ou, J. H., Masiarz, F., Kan, Y. W., Goldfine, I. D., Roth, R. A., and Rutter, W. J. (1985) *Cell 40*, 747−758.
7. Ullrich, A., Bell, J. R., Chen, E. Y., Herrera, R., Petruzelli, L. M., Dull, T. J., Gray, A., Coussens, L., Liao, Y.-C., Tsubokowa, M., Mason, A., Seeburg, P. H., Grunfeld, C., Rosen, O. M., and Ramachandran, J. (1985) *Nature 313*, 756−761.
8. White, M. F., and Kahn, R. (1994) *J. Biol. Chem. 269*, 1−4.
9. Fantl, W. J., Johnson, D. E., and William, L. T. (1993) *Annu. Rev. Biochem. 62*, 453−481.
10. Deller, M. C., and Jones, E. Y. (2000) *Curr. Opin. Struct. Biol. 10*, 213−219.
11. Taylor, R. (1991) *Clin. Endocrinol. (Oxford) 34*, 159−171.
12. Ueno, H., Colbert, H., Escobedo, J. A., and Williams, L. T. (1991) *Science 252*, 844−848.
13. Kashles, O., Yarden, Y., Fischer, R., Ullrich, A., and Schlessinger, J. (1991) *Mol. Cell. Biol. 11*, 1454−1463.
14. Ullrich, A., and Schlessinger, J. (1990) *Cell 61*, 203−212.
15. Ueno, H., Gunn, M., Dell, K., Tseng, A., Jr., and William, L. T. (1992) *J. Biol. Chem. 267*, 1470−1476.
16. Bellot, F., Crumley, G., Kaplow, J. M., Schessinger, J., Jaye, M., and Dionne, C. A. (1991) *EMBO J. 10*, 2849−2854.
17. Plotnikov, A. N., Schlessinger, J., Hubbard, S. R., and Mohammadi, M. (1999) *Cell 98*, 641−650.
18. Stauber, D. J., DiGariele, A. D., and Hendrickson, W. A. (2000) *Proc. Natl. Acad. Sci. U.S.A. 97*, 49−54.
19. Mongkolsapaya, J., Grimes, J. M., Chen, N., Xu, X. N., Stuart, D. I., Jones, E. Y., and Screaton, G. R. (1999) *Nat. Struct. Biol. 6*, 1048−1053.
20. Hymowitz, S. G., Christinger, H. W., Fuh, G., Ultsch, M., O'Connel, M., Kelley, R. F., Ashkenazi, A., and de Vos, A. M. (1999) *Mol. Cell 4*, 563−571.
21. Taylor, S. I., Cama, A., Accili, D., Farbetti, F., Quon, M. J., De La Luz Sierra, M., Suzuki, Y., Koller, E., Levy-Toledano, R., Wertheimer, E., Mancada, V. Y., Kadowaki, H., and Kodawaki, T. (1992) *Endocr. Rev. 13*, 566−595.
22. Hubbard, S. R., Wei, L., Ellis, L., and Henderson, W. A. (1994) *Nature 372*, 746−754.
23. Hubbard, S. R. (1997) *EMBO J. 16*, 5572−5581.
24. Casasnovas, J. M., Springer, T. A., Liu, J. H., Harrison, S. C., and Wang, J. H. (1997) *Nature 387*, 312−315.
25. Copie, V., Tomita, Y., Akiyama, S. K., Aota, S., Yamada, K. M., Venable, R. M., Pastor, R. W., Krueger, S., and Torchia, D. A. (1998) *J. Mol. Biol. 277*, 663−682.
26. Garrett, T. P. J., McKern, N. M., Lou, M., Frenkel, M. J., Bentley, J. D., Lovrecz, G. O., Ellerman, T. C., Cosgrove, L. J., and Ward, C. W. (1998) *Nature 394*, 395−399.
27. Moran, M. E., Koch, C. A., Anderson, D., Ellis, C., England, L., Martin, G. S., and Pawson, T. (1990) *Proc. Natl. Acad. Sci U.S.A. 87*, 8622−8626.
28. White, M. F. (1994) *Curr. Opin. Genet. Dev. 4*, 47−54.
29. Okada, T., Kamano, Y., Sakakibara, T., Hazeki, O., and Ui, M. (1994) *J. Biol. Chem. 269*, 3568−3573.
30. Cheatham, B., Vlahos, C. J., Cheatham, L., Wang, L., Blenis, J., and Kahn, C. R. (1994) *Mol. Cell. Biol. 14*, 4902−4911.
31. Kahn, C. R., and White, M. F. (1988) *J. Clin. Invest. 82*, 1551−1556.
32. Dent, P., Lavoinne, A., Nakielny, S., Caudwell, F. B., Watt, P., and Cohen, P. (1990) *Nature 348*, 302−307.
33. King, H., and Rewers, M. (1993) *Diabetes Care 16*, 137−177.
34. Withers, D. J., and White, M. (2000) The Insulin signaling system—A common link in the pathogenesis of type 2 diabetes, *Endocrinology 141*, 1917−1921.
35. Marino-Buslje, C., Mizuguchi, K., Siddle, K., and Blundell, T. L. (1990) *FEBS Lett. 441*, 331−336.
36. Schaefer, E. M., Erickson, H. P., Federwisch, M., Wollmer, A., and Ellis, L. (1992) *J. Biol. Chem. 267*, 23393−23402.
37. Woldin, C. N., Hing, F. S., Lee, J., Pilch, P. F., and Shipley, G. G. (1999) *J. Biol. Chem. 274*, 34981−34992.
38. Tulloch, P. A., Lawrence, L. J., McKern, N. M., Robinson, C. P., Bentley, J. D., Cosgrove, L., Ivancic, N., Lovrecz, G. O., Siddle, K., and Ward, C. W. (1999) *J. Struct. Biol. 125*, 11−18.
39. Murray-Rust, J., NcLeod, A. N., Blundell, T. L., and Wood, S. P. (1992) *BioEssays 14*, 325−331.
40. Sparrow, L. G., McKern, N. M., Gorman, J. J., Strike, P. M., Robinson, C. P., Bentley, J. D., and Ward, C. W. (1997) *J. Biol. Chem. 272*, 29460−29467.
41. Kristensen, C., Wiberg, F. C., Schaffer, L., and Andersen, A. S. (1998) *J. Biol. Chem. 273*, 17780−17786.
42. Mynarcik, D. C., Williams, P. F., Schaffer, L., Yu, G. Q., and Whittaker, J. (1997) *J. Biol. Chem. 272*, 18650−18655.
43. Molina, L., Marino-Buslje, C., Quinn, D. R., and Siddle, K. (2000) *FEBS Lett. 467*, 226−230.
44. Mulhern, T. D., Brooker, G. W., and Cosgrove, L. A. (1998) *Trends Biochem. Sci. 23*, 465−466.
45. Zhang, B., and Roth, R. A. (1991) *Proc. Natl. Acad. Sci. U.S.A. 88*, 9858−9862.
46. Livnah, O., Stura, E. A., Middleton, S. A., Johnson, D. L., Jolliffe, L. K., and Wilson, I. A. (1999) *Science 283*, 987−990.
47. Rigby, A. C., Barber, K. R., Shaw, G. S., and Grant, C. W. (1996) *Biochemistry 35*, 12591−12601.
48. Yip, C. C. (1992) *J. Cell. Biochem. 48*, 19−25.
49. De Meyts, P., Gu, J. L., Shymko, R. M., Kaplan, B. E., Bell, G. I., and Whittaker, J. (1990) *Mol. Endocrinol. 4*, 409−416.
50. Schwartz, G. P., Burke, G. T., and Katsoyannis, P. G. (1989) *Proc. Natl. Acad. Sci. U.S.A. 86*, 458−461.
51. Conlon, J. M., Cavanaugh, E. S., Mynarcyk, D. C., and Whittaker, J. (1996) *Biochem. J. 313*, 283−287.
52. Zimmerman, A. E., Moule, M. L., and Yip, C. C. (1974) *J. Biol. Chem. 249*, 4026−4029.

53. Boni−Schnetzler, M., Scott, W., Waugh, S. M., DiBella, E., and Pilch, P. F. (1987) *J. Biol. Chem. 262*, 8395−8401.
54. Sung, C. K., Wong, K. Y., Yip, C. C., Hawley, D. M., and Goldfine, I. D. (1994) *Mol. Endocrinol. 8*, 315−324.
55. Shoelson, S. E., White, M. F., and Kahn, C. R. (1988) *J. Biol. Chem. 263*, 4852−4860.
56. De Meyts, P., Roth, J., Neville, D. M., Jr., Gavin, J. R., III, and Lesniak, M. A. (1973) *Biochem. Biophys. Res. Commun. 55*, 154−161.
57. Yip, C. C., Hsu, H., Patel, R. G., Hawley, D. M., Maddux, B. A., and Goldfine, I. D. (1988) *Biochem. Biophys. Res. Commun. 157*, 321−329.
58. Grunberger, G., Zick, Y., and Gorden, P. (1984) *Science 223*, 932−934.
59. Roach, P., Arakaki, R. F., Accili, D., and Taylor, S. I. (1992) *Clin. Res. 40*, 311A.
60. Kahn, R. C., White, M. F., Shoelson, S. E., Backer, J. M., Araki, E., Cheatham, B., Csermely, P., Folli, F., Goldstein, B. J., Huertas, P., Rothenberg, P. L., Saad, M. J. A., Siddle, K., Sun, X.-J., Wilden, P. A., Yamada, K., and Kahn, S. A. (1993) *Recent Prog. Hormone Res. 48*, 291−339.
61. Lee, J., and Pilch, P. F. (1994) *Am. J. Physiol. 266*, C319−C334.
62. Frattali, A. L., Treadway, J. L., and Pessin, J. E. (1991) *J. Biol. Chem. 266*, 9829−9834.
63. Longo, N., Shuster, R. C., Griffin, L. D., Langley, S. D., and Elsas, L. J. (1992) *J. Biol. Chem. 267*, 12416−12419.
64. Boni-Schnetzler, M., Rubin, J. B., and Pilch, P. F. (1986) *J. Biol. Chem. 261*, 15281−15287.
65. Smith, G. D., Ciszak, E., and Pangborn, W. (1996) *Protein Sci. 5*, 1502−1511.
66. Leahy, D. J., Aukhil, I., and Erickson, H. P. (1996) *Cell 84*, 155−164.

BI0015921